Chemistry Faculty Publications   Chemistry

7-2010

Synthesis Of Pbs/tio2 Colloidal Heterostructures For Photovoltaic Applications

Krishna P. Acharya

Nishshanka N. Hewa-Kasakarage

Taiwo R. Alabi

Ian Nemitz

Elena Khon

See next page for additional authors

Repository Citation

Acharya, Krishna P.; Hewa-Kasakarage, Nishshanka N.; Alabi, Taiwo R.; Nemitz, Ian; Khon, Elena; Ullrich, Bruno; Anzenbacher, Pavel Jr.; and Zamkov, Mikhail, "Synthesis Of Pbs/tio2 Colloidal Heterostructures For Photovoltaic Applications" (2010). *Chemistry Faculty Publications*. 53.
https://scholarworks.bgsu.edu/chem_pub/53

Author(s)

Krishna P. Acharya, Nishshanka N. Hewa-Kasakarage, Taiwo R. Alabi, Ian Nemitz, Elena Khon, Bruno Ullrich, Pavel Anzenbacher Jr., and Mikhail Zamkov

Synthesis of PbS/TiO₂ Colloidal Heterostructures for Photovoltaic Applications

Krishna P. Acharya,[†,§] **Nishshanka N. Hewa-Kasakarage,**[§] **Taiwo R. Alabi,**[†,§] **Ian Nemitz,**[§] **Elena Khon,**[†,§] **Bruno Ullrich,**[†,§] **Pavel Anzenbacher,**[†,‡] **and Mikhail Zamkov**[*,†,§]

The Center for Photochemical Sciences and Departments of Chemistry and Physics and Astronomy, Bowling Green State University, Bowling Green, Ohio 43403

Received: May 08, 2010; Revised Manuscript Received: June 16, 2010

We report on heteroepitaxial growth of nearly monodisperse PbS nanocrystals onto the surface of TiO₂ nanoparticles via colloidal hot-injection routes. Fabricated PbS/TiO₂ nanocomposites can be dispersed in nonpolar solvents, which enables an easy solution processing of these materials into mesoporous films for use as light-absorbing layers in nanocrystal-sensitized solar cells. High-temperature deposition of the sensitizer material allows controlling both the size and the number of PbS domains grown onto TiO₂ nanoparticles, whereby providing synthetic means for tuning the absorbance spectrum of PbS/TiO₂ nanocomposites and simultaneously enhancing their photocatalytic response in the visible and near-infrared. Compared with conventional ionic bath deposition of PbS semiconductors onto TiO₂, the reported method results in an improved nanocrystal quality and narrower distribution of PbS sizes; meanwhile, the use of hot-temperature deposition of PbS (*T* = 180 °C) promotes the formation of near-epitaxial relationships between PbS and TiO₂ domains, leading to fewer interfacial defects. The photovoltaic response of pyridine-treated PbS/TiO₂ nanocomposites was investigated using a two-electrode cell filled with polysulfide electrolyte. The measured photocurrent compared favorably to that of PbS/TiO₂ electrodes fabricated via chemical bath deposition.

1. Introduction

Semiconductor nanocrystals (NCs) represent a promising class of nanomaterials for the development of new-generation solar cells because of the superior optoelectronic properties of inorganic semiconductors and the stability of as-prepared nanocrystals in colloidal suspensions, which allows for inexpensive, solution-based device fabrication. The demonstrated potential of these materials for the enhanced absorption of solar light and efficient charge separation has given rise to several photovoltaic architectures, including hybrid bulk hetero-junction,[1–15] all-inorganic,[16–23] and nanocrystal-sensitized[24–40] solar cells. For instance, spin-coated films of semiconductor NCs can be introduced as light-absorbing layers and simultaneously as n-type components in nanocrystal/polymer bulk heterojunction solar cells, or, alternatively, incorporated into an all-inorganic bilayer design comprising a heterojunction of n- and p-type NC films. The benefits of using semiconductor NCs in mesoscopic solar cells are readily apparent through a superior thermal stability of these devices and improved solar extinction coefficients; nevertheless, the present day conversion efficiencies of NC-based cells remain relatively low, which has been attributed to the inefficient intraparticle conductance of photogenerated charges through a 3D matrix of organic-coated nanocrystals.[41–46]

The problem of poor carrier collection in NC-based solar cells can be avoided if colloidal NCs are excluded from the process of carrier transport and participate primarily as inorganic light-absorbing elements. This type of light-harvesting mechanism has been successfully implemented in the past through a dye-sensitized solar cell design,[47] where semiconductor NCs were employed as light sensitizers in lieu of organic dyes.[36] The transport of photogenerated electrons toward a working electrode, in this case, is mediated via mesoporous TiO₂, whereas photoinduced holes are regenerated by means of a liquid[48–50] or solid[40,51] electrolyte. From the long-term prospective, the attempted replacement of organic sensitizers with inorganic semiconductor NCs in dye-sensitized solar cells constitutes a natural step toward increasing the intake of solar energy and improving the system's long-term stability against photodegradation but may require further development of the donor–acceptor architecture, as highlighted by a number of recent investigations.[24–36,52]

At present, there are two main schemes for the deposition of NC sensitizers onto the surface of TiO₂, which include (i) introducing organic linker-molecules that bridge colloidal NCs with TiO₂ and (ii) growing NCs directly onto the oxide surface via chemical bath deposition (CBD) or successive ionic layer adsorption and reaction (SILAR) process.[53] The former approach has been successfully employed to couple CdS,[54] CdSe,[31,55,56] InAs,[35] PbSe,[57] and PbS[58] NCs onto TiO₂ via 3-mercaptopropionic acid (MPA) or through a nonepitaxial contact to organic ligands and, thus far, has yielded up to 1.7%[35] of power conversion efficiency (PCE). The main drawback of this method is considered to be the presence of organic spacers between nanocrystal and oxide domains, which augment the tunneling barrier between excited states of a sensitizer and the conduction band of TiO₂, causing a decrease in electron transfer probability. In addition, a number of experimental works have demonstrated that organic linkers can also serve as carrier traps, which further reduce the electron transfer rate. These drawbacks, associated mainly with the presence of organic linkers in the NC-TiO₂ assembly, are successfully avoided in the second deposition method, where NCs are grown directly on TiO₂ via CBD,[26,27,36,37,39,59,60] leading to all-inorganic NC/TiO₂ heterostructures. Indeed,

* Corresponding author. E-mail: zamkovm@bgsu.edu.
† The Center for Photochemical Sciences.
‡ Department of Chemistry.
§ Department of Physics and Astronomy.

Synthesis of PbS/TiO₂ Colloidal Heterostructures

J. Phys. Chem. C, Vol. 114, No. 29, 2010 **12497**

recent studies have shown that CBD-grown NC/oxides films show an improved carrier injection and superior PCE and incident photon to current efficiency (IPCE) values.[61] The quality and the size distribution of CBD-grown NC sensitizers, however, remain inferior to those synthesized through colloidal techniques.[62] Furthermore, the aqueous route to growing of NC sensitizers through CBD approach is often ineffective with air-sensitive semiconductors, such as PbSe or PbS, as revealed by an overall low crystallinity of these materials.[36]

Here we demonstrate a facile method for developing PbS-sensitized TiO₂ films, which combines the benefits of the hot-injection colloidal route to the synthesis of monodisperse PbS NC sensitizers, with the advantages of linker-free, all-inorganic, PbS/TiO₂ heterojunction. In the present approach, the processes of sensitizer deposition and sintering of the film are performed in the reverse chronological order, which allows for a high-temperature growth of the PbS sensitizer directly onto the surface of TiO₂, followed by a solution-phase deposition of PbS-modified TiO₂ nanoparticles (NPs) onto a conductive substrate. The resulting PbS/TiO₂ films are then subjected to high-temperature annealing to remove residual surface ligands, whereby yielding an all-inorganic absorbing layer. In light of the renewed interest in NC-sensitized solar cells, which revival is fueled by the ongoing research and discovery of noncorrosive,[40,63,64] and longer-lasting[50] hole-scavenging materials, the PbS/TiO₂ heterostructured films reported here could potentially lead to high-efficiency NC-sensitized solar cells.

Recently, colloidal growth of heteroepitaxial semiconductor/TiO₂ composites via hot-injection routes has been demonstrated by several groups.[65,66] Acharya et al.[66] has reported the synthesis of PbSe/TiO₂ nanostructures, comprising near-epitaxial assemblies of PbSe NCs and TiO₂ nanorods (NRs), where the average size of NC sensitizer could be tuned from 2 to 5 nm. Unfortunately, a relatively low position of the conduction band edge in PbSe NCs prevented the desirable combination of a narrow-band gap PbSe sensitizer and proper alignment of PbSe and TiO₂ excited state levels needed for an efficient electron transfer. In contrast with PbSe/TiO₂ heterostructures, the PbS/TiO₂ combination of materials, explored in this work, supports the PbS-to-TiO₂ electron transfer even for large diameter PbS NCs[58] ($d \approx 7$ nm), which allows obtaining a near-optimum range of band gap energies for the solar energy conversion ($\hbar\omega \approx$ 1.0 to 1.4 eV). Here we demonstrate a controlled tuning of PbS domain sizes in the 2−20 nm range with an average dispersion of PbS diameters between 9 and 14%. Owing to a sequential two-step approach to the synthesis of TiO₂/PbS NCs, the size and the shape of TiO₂ domains can be tuned as well, which provides an additional avenue for optimizing the transport of photoinduced carriers through an array of TiO₂/PbS NPs.

Following the purification step, colloidal suspensions of synthesized PbS/TiO₂ NCs were used to fabricate ethanol-based pastes for the development of thin films on top of a conductive transparent electrode. After annealing, these films were incorporated into a standard two-electrode cell filled with polysulfide electrolyte for electrochemical characterization. The measured photoaction spectra compared favorably to those of PbS/TiO₂ films fabricated via conventional CBD route.

2. Experimental Section

2.1. Materials. 1-Octadecene (ODE, 90% Aldrich), oleylamine (OLAM, 70% Aldrich), oleic acid (OA, 90% Aldrich), titanium tetrachloride (TiCl4, 99.9% Aldrich), titanium(IV) isopropoxide (99.999%, Aldrich), ethanol (anhydrous, 95% Aldrich), pyridine (anhydrous, 99.8% Aldrich), lead(II) nitrate (99.99%, Aldrich), lead(II) oxide powder (PbO, 99.999% Aldrich), chloroplatinic acid hydrate (99.9%, Aldrich), sodium sulfide nonanhydrate (98%, Alfa Aesar), sulfur (99.999%, Acros), 2-propanol (99.8%, Acros), ITO/glass (8−12 ohm/sq, Aldrich), and titanium dioxide (P25, Evonick Degussa) were used as received without any further purification. All reactions were performed under argon atmosphere using the standard Schlenk technique.

2.2. Preparation of Injection Precursors. We prepared the lead precursor by dissolving 0.8 g (3.5 mmol) of lead oxide in a mixture of 1.3 g of OA and 4 g of ODE via heating the flask to 200 °C for 30 min. Prior to the injection, the temperature of the Pb solution was lowered to 140 °C. A sulfur solution was prepared by dissolving 0.10 g (3.1 mmol) of S in 2.4 g of ODE at 200 °C for 5 min. The solution was subsequently cooled to the room temperature.

2.3. Synthesis of PbS/TiO₂ Heterostructures. One-pot synthesis of PbS/TiO₂ nanocomposites proceeded via the initial growth of TiO₂ NRs, onto which PbS NCs were subsequently grown by injecting lead and sulfur precursors at lower temperatures. To fabricate TiO₂ NRs, 2.85 g OLAM and 0.28 g OLAC were mixed in a three-necked flask and degassed using mechanical vacuum pump at 120 °C for 30 min.[67] The mixture was subsequently switched to argon, and 0.05 mL (0.45 mmol) of TiCl₄ was injected into the flask at 40 °C. The reaction mixture was then heated to 300 °C and kept at that temperature for 30 min. For the growth of 3 to 4 nm PbS NCs, the temperature of the reaction mixture was lowered to 180 °C, and the full amount of both precursors Pb (at $T = 180$ °C) and S (at room temperature) was simultaneously injected under vigorous stirring. The initial 40−50 °C drop in the temperature of the solution recovered to 180 °C within 2 min, whereas the solution color turned dark almost immediately after injection. We stopped the reaction after 2 min by removing the flask from the heating mantle, at which point 6 mL of degassed toluene was added. Cleaning of NPs was performed by a repetitive precipitation in ethanol and a subsequent redissolution in toluene. For the last cleaning cycle, the precipitation was done using a mixture of ethanol and toluene (1:8 by volume) to remove any isolated nanocrystals in the mixture.

2.4. PbS/TiO₂ (Nanocomposite) and PbS/TiO₂ (P25-CBD) Working Electrode Preparation. Prior to the development of nanocomposite films, the bulky ligands on PbS/TiO₂ heterostructures were exchanged with shorter pyridine molecules. For this purpose, PbS/TiO₂ colloids were precipitated with ethanol, redispersed in 8 mL of pyridine, and stirred at 60 °C overnight (15 h). Pyridine-coated PbS/TiO₂ nanocomposites were subsequently precipitated, mixed with a few drops of ethanol, and sonicated for 50 min to a get homogeneous paste. A thin film was then spread onto ITO/glass substrate using a doctor blade method over the area of ∼60 mm². (See the insert in Figure 7b.) The sintering was performed on a hot plate under argon flow. To fabricate a working electrode using a CBD method, 1.75 g of TiO₂ NPs (Degussa, P25) was mixed with 7.5 mL ethanol and sonicated for 40 min. Subsequently, 0.25 mL of titanium tetraisopropoxide was added, and the mixture was sonicated further to form a homogeneous paste. After the deposition of TiO₂ (P25) film onto ITO covered glass, it was sintered at 450 °C for 30 min to allow good electronic conduction.[68] In situ deposition of PbS on TiO₂ was carried out in the chemical bath of the precursor material through a SILAR process.[69] For this purpose, TiO₂ working electrode film was immersed in 0.02 M methanol solution of Pb(NO₃)₂ for 1 min,

rinsed with methanol, followed by immersing in 0.02 M methanol Na$_2$S solution for 1 min, and rinsed again with methanol, making one complete deposition cycle. This process was repeated six times and was monitored by recording absorbance spectra at each step. (See Figure SF5 of the Supporting Information.)

2.5. Assembly of PbS/TiO$_2$ Solar Cells and Photocurrent Measurements. Polysulfide electrolyte was made by combining 0.5 M Na$_2$S, 1.5 M sulfur, and 0.2 M KCl in methanol and water (7:3).[70] We prepared platinized ITO counter electrode by spreading few drops of 5 mM chloroplatinic acid in 2-propanol on the glass, followed by heating to 400 °C for 1 h. A parafilm spacer with a central opening was put on the top of the film and filled with a few drops of electrolyte. The assembly of the cell was completed by capping the device with a platinized ITO/glass counter electrode. Photocurrent (PC) spectra were measured using a lock-in amplifier (SR830). The device was illuminated through the working electrode side using a xenon lamp, output of which was dispersed in a monochromator and chopped with a frequency of 15 Hz. (For the dependence of the measured PC on the chopper frequency, see Figure SF6 of the Supporting Information.) The excitation area was ~4 mm^2 with excitation power of ~0.25 μW/mm^2 (at λ = 420 nm).

2.6. Characterization. UV–vis absorption and photoluminescence spectra were recorded using CARY 50 scan spectrophotometer, Simadzu UV-3600 UV–vis-NIR spectrophotometer, and Jobin Yvon Fluorolog FL3-11 fluorescence spectrophotometer. High-resolution transmission electron microscopy (TEM) measurements were carried out using a JEOL 3011UHR apparatus, operated at 300 kV. High angular annular dark field scanning TEM was performed using JEOL 2010 transmission electron microscope. Specimens were prepared by depositing a drop of nanocrystal toluene solution onto a carbon-coated copper grid and letting it dry in air. X-ray powder diffraction (XRD) measurements were carried out on a Scintag XDS-2000 X-ray powder diffractometer. Scanning electron micrograph was taken using a Inspect F scanning electron microscope (SEM), and energy dispersive X-ray (EDX) emission spectra were measured using an EDAX X-ray detector located inside the SEM. The electron beam was accelerated at 10 kV.

2.7. Fluorescence Lifetime Measurements. FL lifetime measurements were performed using a time-correlated single-photon counting setup utilizing SPC-630 single-photon counting PCI card (Becker & Hickle GmbH), picosecond diode laser operating at 400 nm, as an excitation source (Picoquant), and id50 avalanche photodiode (Quantique). The repetition rate of the laser was chosen to allow for a 1000 ns time window, whereas the pulse fluence was adjusted to produce about 1 emission photon per 100 excitation pulses (excitation power was 70 μW).

3. Results and Discussion

The shape of the composite nano-object forming as a result of solution-phase coupling of the two structurally dissimilar materials is determined by the interplay between the total surface energy of the composite structure and the solid–solid interfacial energy, which is related to the mismatch-induced strain between the two merging lattices. If the interfacial strain is low, then the two materials can be joined epitaxially over large surface areas, using, for instance, standard methods of chemical and physical vapor deposition. In the case when the interfacial strain exceeds the surface tension of both domains, the uniform and continuous growth of material layers is no longer possible.

Instead, the composite structure undergoes a spatial rearrangement that eliminates some of the interfacial region by increasing the overall surface area.[71] Such growth mechanism has been previously observed for PbS/TiO$_2$ heterostructures, fabricated via CBD route, where the formation of island-like PbS domains was apparent.[40] Because of the lack of synthetic means for controlling the surface tension of growing PbS NCs within the CBD approach, it was generally impossible to achieve a narrow distribution of PbS diameters.

A colloidal, nonaqueous approach to the synthesis of heterostructured materials provides an additional degree of freedom for controlling the shape of composite NPs, associated with the presence of surface-passivating ligands that modulate the surface tension of growing crystallites. By optimizing the type and the concentration of ligand molecules in the growth solution, it is often possible to accommodate the misfit-induced interfacial strain between the two semiconductor materials and to coerce the narrow size distribution of growing domains. Here we explore the effect of various ligand combinations as well as their concentrations on the overall shape of PbS/TiO$_2$ heterostructures, specifically targeting those synthetic conditions that lead to the narrow distribution of PbS diameters. In a typical procedure, the PbS deposition step is performed using a combination of OA and OLAM ligands dispersed in ODE. (See the Experimental Section.) By employing a binary mixture of stabilizing ligands (OA and OLAM), we were able to control independently the strength and the concentration of surface molecules on PbS NCs. Here we explored the effect of surface passivation on the shape of PbS NCs by conducting a series of experiments utilizing different concentrations of OA and OLAM surfactants. We achieved further tuning of the PbS NP shape by optimizing the concentrations of Pb and S precursors in the growth solution containing a fixed amount of TiO$_2$ NPs.

Figure 1 shows typical TEM images of PbS/TiO$_2$ heterostructures fabricated under various synthetic conditions. A careful analysis of PbS/TiO$_2$ shapes reveals that the formation of small- and large-diameter PbS NCs on the surface of TiO$_2$ occurs via two independent mechanisms. For instance, smaller-size PbS "islands" ranging from 2 to 4 nm in diameter (see Figure SF1 of the Supporting Information for the statistical distributions of sizes) tend to be symmetrically distributed throughout the surface of NRs. Such uniform coverage of PbS NCs on TiO$_2$ can be explained in terms of fundamental energy requirements on the deposition of the secondary material in heteroepitaxial growth. Namely, the spatially isotropic addition of PbS monomers onto TiO$_2$ NRs initially results in the formation of a thin PbS shell, which can be identified in structures sampled at intermediate steps (see Figure SF2a of the Supporting Information) through a combination of TEM and energy dispersive X-ray (EDX) analyses. A subsequent lateral expansion of this shell causes a mismatch-induced increase in the interfacial energy and, therefore, promotes the collapse of the PbS layer into segregated islands.

Whereas the coalescence of the PbS shell into evenly distributed dot-shaped domains seems to be consistent with the structural appearance of small-diameter PbS on TiO$_2$ (see, for example, Figure 1a,d), this process cannot explain the formation of large-diameter PbS NCs that tend to grow only at specific locations along the TiO$_2$ surface. Strong evidence supporting the independent growth mechanism in this case is provided by the fact that the formation of large-diameter PbS NCs can occur simultaneously with smaller PbS NCs, as seen in high-resolution TEM (Figure SF2c of the Supporting Information) and high angular annular dark-field scanning transmission electron mi-
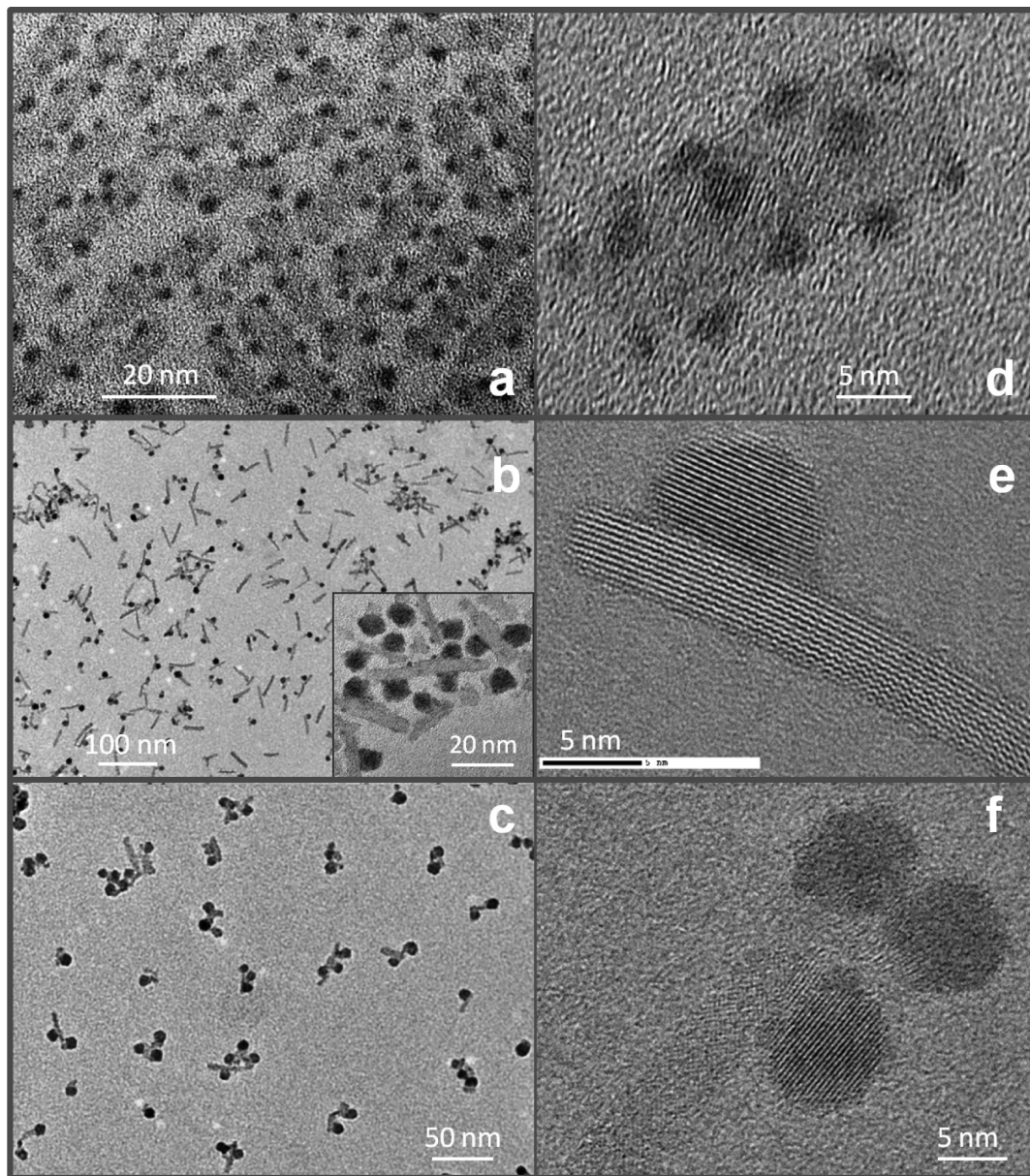
Synthesis of PbS/TiO₂ Colloidal Heterostructures

J. Phys. Chem. C, Vol. 114, No. 29, 2010 **12499**

Figure 1. TEM images of PbS/TiO$_2$ nanocomposites fabricated under various synthetic conditions. (a) High concentration of OA in the growth solution results in the formation of small-diameter ($d < 3$ nm) PbS domains. (b) The formation of single, large-diameter PbS NCs ($d > 4$) is dominant when the concentration of OA in the solution is low. (See the text for details.) (c) The formation of multiple large-diameter PbS NCs per single nanorod occurs when the concentration of OA is low, whereas concentrations of Pb and S precursors are high. (d−f) High-resolution TEM images of nanocomposites shown in (a−c), respectively.

croscopy (HAADF-STEM) images of mixed heterostructures, and the fact that in contrast with small-diameter PbS, the growth rate of larger PbS NCs is strongly correlated with the concentration of Pb and S precursor in the solution. On the basis of these observations, we conclude that larger PbS NCs form at locations of lower interfacial stress, which would allow for near-epitaxial relationships at the PbS/TiO$_2$ boundary and the ensuing low-energy expansion of the PbS lattice. These locations are likely to contain irregularities of the TiO$_2$ lattice that promote a preferential merging of 001 and 100 faces of anatase TiO$_2$ and rock-salt PbS crystal lattices (Figure SF2d of the Supporting Information), which otherwise correspond to a substantial 6.9% lattice mismatch.

Suppression or enhancement of a specific PbS deposition mode, described above, can be achieved by varying the concentration of oleic acid in the growth solution. Typically, the formation of large diameter PbS NCs is favored when the

molar ratio of OA (used for the dissolution of Pb precursor) to ODE is <0.2 and the ratio of PbO to ODE is at least 0.25. Lowering the concentration of OA for a fixed amount of PbO below OA/ODE = 0.2 leads to a significant drop in the actual concentration of OA in the solution due to the formation of Pb−oleate complexes, which results in the growth of large PbS structures that tend to encase TiO$_2$ NPs within their volume. (See Figure SF3 of the Supporting Information.) A similar structural type of PbS/TiO$_2$ nanocomposites can also be formed when the amount of PbO is increased with respect to OA (molar ratio of PbO/OA > 1.5), which depletes the amount of desorbed OA molecules in the solution. If the concentration of OA is high (OA/ODE >0.2), then the growth of large-diameter PbS domains is suppressed, and the formation of small, uniformly distributed PbS domains becomes dominant (Figure 1a).

A ligand-induced control over the shape of growing nano-crystals can also be applied to oxide domains of PbS/TiO$_2$
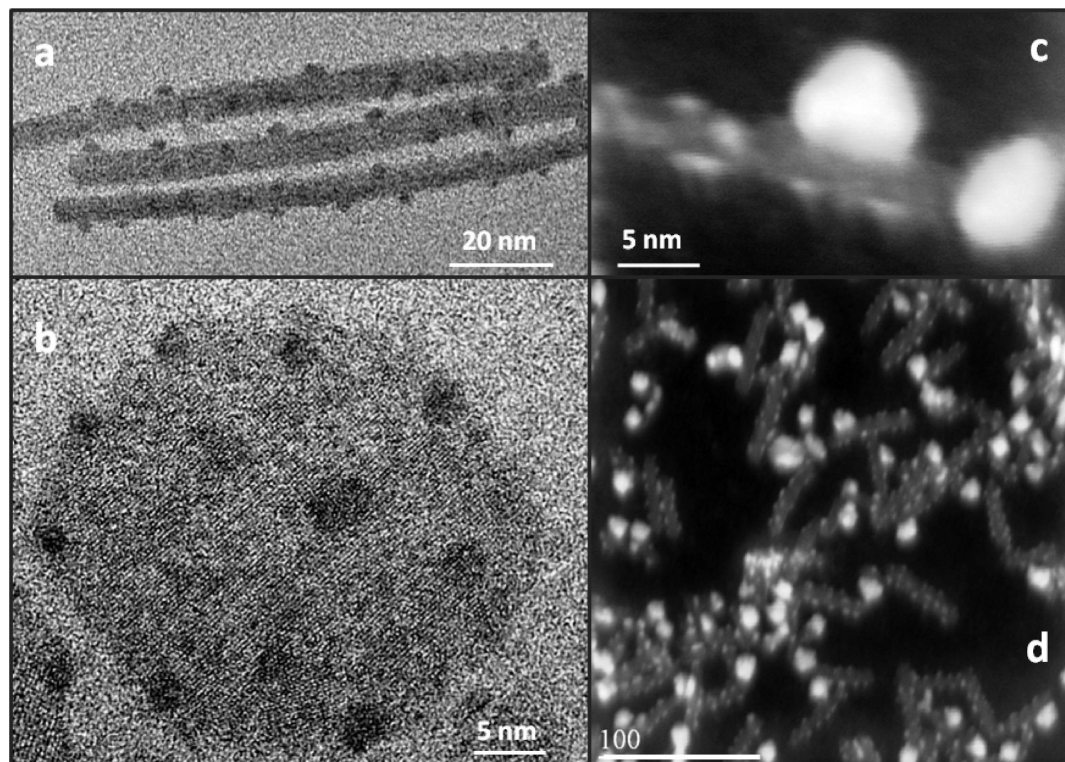
Figure 2. (a,b) TEM images of PbS/TiO$_2$ superstructures self-assembled from PbS/TiO$_2$ nanocomposites either through (a) longitudinal or (b) lateral attachment of TiO$_2$ domains. (c,d) HAADF-STEM images of PbS/TiO$_2$ heterostructures comprising both small ($d = 2.2$ nm) and large ($d = 7.1$ nm) PbS NCs.

nanocomposites. For instance, in the first stage of the synthesis, the shape of TiO$_2$ NRs is only weakly affected, even by strong variations (up to 300%) in the relative molar ratio of stabilizing agents (OA/OLAM). However, during the PbS deposition step, a small reduction in the concentration of injected OA (added during the precursor injection) to that of OLAM (OA/OLAM < 0.3) can enable a coalescence of PbS/TiO$_2$ heterostructures either via longitudinal or lateral attachment of NR domains. Examples of both are shown in Figure 2a,b. The observed merging of PbS/TiO$_2$ heterostructures via coupling of TiO$_2$ domains increases the average size of TiO$_2$ NPs in the sample and could be employed for the development of NCs films with large-grain sizes, potentially matching those of commercially available TiO$_2$ pastes (e.g., Merck or Degussa), fabricated via aqueous routes.

Further structural analysis of PbS/TiO$_2$ nanocomposites comprising 4.2 nm diameter PbS NCs was performed using a combination of XRD and EDX techniques (Figure 3). For this purpose, the samples were repeatedly washed to remove any unreacted precursors and finally precipitated in the form of NC powder. A typical EDX spectrum in Figure 3a confirms the presence of Pb, Ti, S, and O elements in grown nanocomposites, whereas XRD measurements (Figure 3b) indicate the existence of both PbS (rock-salt) and TiO$_2$ (anatase) crystal structures.

It is expected that optoelectronic properties of PbS/TiO$_2$ heterostructures are strongly dependent on the average size of the PbS domain. According to the excited-state energy diagram[72,73] in Figure 4, a photoinduced electron transfer across PbS/TiO$_2$ interface is energetically allowed only when the diameter of PbS NCs is <7 nm. In this case, the staggered alignment of conduction and valence band edges at the PbS/TiO$_2$ interface creates positive exothermicity that drives the electron transfer reaction. Conversely, for PbS NPs with diameters >7 nm, the PbS/TiO$_2$ heterostructure exhibits type I alignment of band
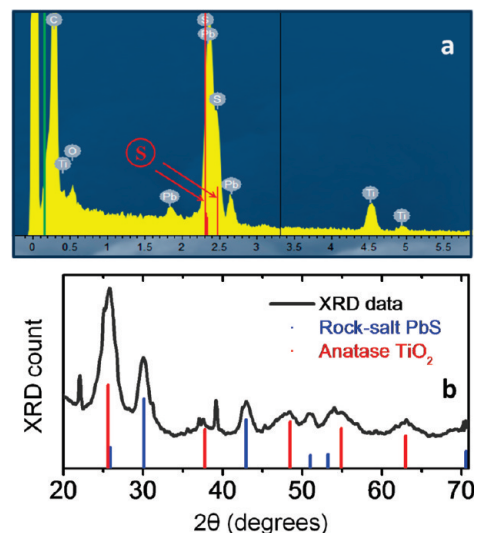

Figure 3. Structural analysis of PbS/TiO$_2$ nanocomposites (with 4.2 nm PbS NCs) using EDX and XRD techniques. (a) A typical EDX scan of a PbS/TiO$_2$ nanoparticle film confirming the presence of Pb, S, Ti, and O elements in fabricated materials. (b) A typical XRD spectrum of PbS/TiO$_2$ nanoparticle powder showing characteristic Bragg lines indexed to the rock-salt PbS and anatase TiO$_2$ crystal lattices.

edges, in which case both excited carriers remain within the PbS material.

The size-dependent alignment of energy levels in PbS/TiO$_2$ nanocomposites is reflected in optical properties of these colloids. For instance, the absorption profile of PbS/TiO$_2$ NPs comprising small diameter ($d = 2.3$ nm) PbS NCs is characteristic of type II heterostructures with nonzero photon absorption in the spectral range below the band gap of both PbS (edge at 600 nm) and TiO$_2$ materials. This infrared component arises because of excitations of intermediate states that exist at the
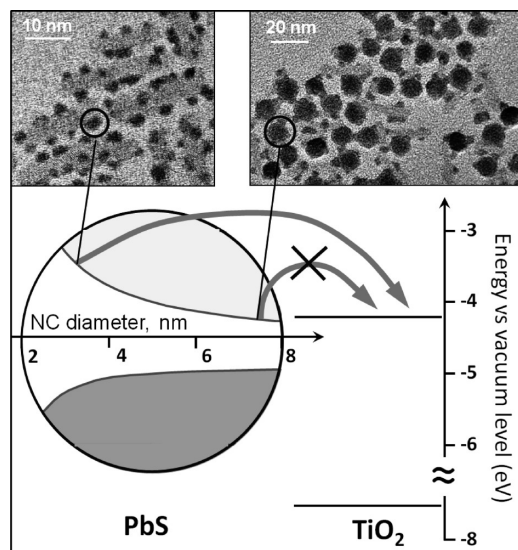
Synthesis of PbS/TiO$_2$ Colloidal Heterostructures

J. Phys. Chem. C, Vol. 114, No. 29, 2010 **12501**

Figure 4. Energy diagram showing a relative alignment of the conduction and valence band edges in PbS/TiO$_2$ heterostructures. According to the expected relationship between the energy of 1S$_e$ (PbS) state and the nanocrystal size, the photoinduced electron transfer from PbS to TiO$_2$ domain is allowed only if the diameter of PbS NCs is <7 nm.

junction of the two domains[74] as well as spatial delocalization of carrier wave functions over quasi-epitaxial heterostructures and is beneficial for photovoltaic applications of these nanocomposites because it red shifts the absorption range of PbS/TiO$_2$ by several hundreds of nanometers. In addition to the infrared tail, the absorption profile in Figure 5b shows a small excitonic peak near 600 nm; its spectral position agrees well with the expected band gap absorption in 2.3 nm PbS NCs. This feature is absent in the spectrum of mixed PbS/TiO$_2$ heterostructures (green curve) possibly due to the overlapping absorption of large-diameter PbS NCs. Likewise, there is no clear indication of band edge transitions in PbS/TiO$_2$ NPs, comprising only large-diameter PbS NCs ($d = 4.2$ nm). The absence of the excitonic peak in the latter case cannot be attributed to the sample inhomogeneity alone because the size dispersion of PbS NCs in these heterostructures is only 12% and is likely to arise from excitations of intermediate states that exist at the interface of PbS and TiO$_2$ domains.

PbS/TiO$_2$ heterostructures comprising small-diameter PbS NCs showed very weak or no fluorescence in the energy range corresponding to 1S(e)-1S(h) carrier recombination, whereas NPs containing larger PbS domains ($d > 4$) generally produced somewhat stronger emission in the near-infrared ($\lambda = 800-1200$ nm). This result is consistent with the prediction that small-diameter PbS are more likely to inject excited carriers into TiO$_2$, leaving only a small fraction of excited population to decay via radiative channels. An example of a typical emission spectrum corresponding to 4.2 nm PbS-modified TiO$_2$ NPs is shown in Figure 5c. A good agreement between the size of PbS NCs and the spectral position of the FL peak provides strong support to the hypothesis that the origin of the emission is the band edge recombination of carriers in PbS NCs and not the decay of surface or interfacial trap states. The corresponding values of the fluorescence lifetime, measured using time-correlated single-photon counting technique (TCSPC), were found to be in the range of 2 to 5 ns, which is substantially shorter than 1 to 1.8 μs reported[75] for isolated PbS NCs. This 500-fold decrease in the lifetime of TiO$_2$-bound PbS NCs is

attributed to the transfer of photoinduced electrons from the conduction edge of PbS NCs into excited states of TiO$_2$ NRs.

For a conventional design of NC-sensitized solar cells, charge collection mechanism relies on the common acceptor domain, often a mesoporous film of TiO$_2$, to harvest photoinduced carriers from multiple sensitizers. In these cells, photoinduced charge separation is followed by the injection of negative carriers into the oxide film, which serves as a low-resistance pathway for carrier migration toward a working electrode. In the case of PbS/TiO$_2$ nanocomposites, fabricated in this work, a flow of carriers toward a working electrode is obstructed by the presence of organic ligands, which passivate the surface of individual TiO$_2$ NRs. To enable carrier conductivity through the PbS/TiO$_2$ matrix, isolated NR domains should be coupled together via epitaxial relationships to form a common conduction path for carrier migration. Such coupling of TiO$_2$ domains has been extensively researched for aqueous TiO$_2$ NPs, where merging is typically achieved by annealing of spincoated or "doctor-bladed" films at 400−450 °C. In the case of organically passivated TiO$_2$ NRs, however, a high-temperature annealing step may result in the adverse contamination of TiO$_2$ NRs and PbS NCs with carbon-based residues, potentially leading to a high density of lattice defects. To minimize the effect of such contamination, long-chain ligands (OA and OLAM) on PbS/TiO$_2$ colloids were replaced with shorter and more volatile pyridine molecules prior to annealing of the film.

The ligand exchange in PbS/TiO$_2$ nanocomposites was performed according to a previously reported procedure[76] by stirring the colloids with pyridine. An apparent reduction in the solution opacity indicated a successful replacement of bulky ligands, at which point the mixture was centrifuged and the precipitate was discarded. After any excessive solvent from the suspension was removed, a small fragment of the residual paste-like precipitate was taken for further examination in TEM. Figure 6 shows typical low-magnification images of pyridine-coated PbS/TiO$_2$ heterostructures, which, upon solvent evaporation, tend to aggregate into micrometer-size "nets". An apparent decrease in the volume of empty spaces between NPs was consistent with the presence of shorter pyridine ligands on nanocrystal surfaces.

To prepare a working electrode, a thin layer of PbS/TiO$_2$ nanocomposites was deposited onto an indium−tin-oxide (ITO) covered glass using a doctor-blade technique and subsequently annealed at 270 °C. We found that without further improvement of developed NP pastes, a good film quality and satisfactory adhesion to the substrate could be achieved only for the case of thin PbS/TiO$_2$ films ($A = 0.25$ at $\lambda = 500$ nm; see Figure SF4 of the Supporting Information), whereas thicker films tended to corrugate (Figure 6d) and partially peel off the substrate after the annealing step. Upon deposition of the film, the ITO electrode was incorporated into a prototype cell comprising a platinum-coated counter electrode and a liquid electrolyte for PC measurements. The illumination of the cell was done through the working electrode side of the device.

Regeneration of holes in PbS sensitizes poses several experimental challenges associated with the rapid corrosion of nanocrystals and irreversible character of electrolytes. Whereas recent studies by M. Grätzel and M. K. Nazeeruddin have identified a few promising redox couples based on solid spiro-OMeTAD [2,20,7,70,-tetrakis(N,N-di-p-methoxyphenylamine)−9[40] and [Co(o-phen)3]$^{2+/3+}$ complex in acetonitrile/ethylene carbonate[64] that show reversible and stable regeneration of holes in PbS NCs, these hole-scavenging materials are still not commercially available. Consequently, the photoaction of
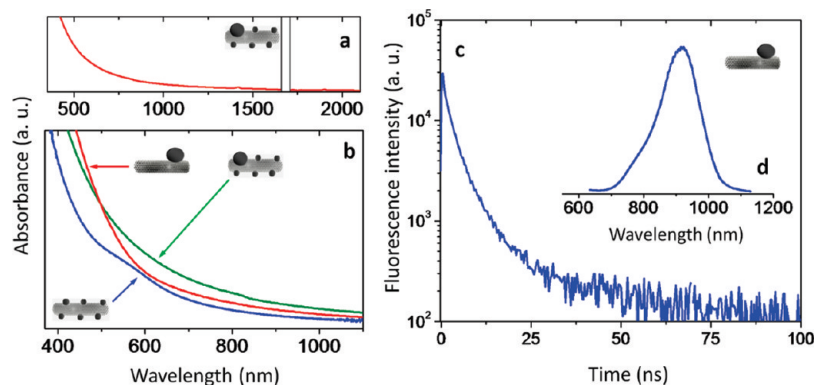
Figure 5. Optical properties of PbS/TiO$_2$ heterostructures. (a–b) Absorbance of PbS/TiO$_2$ nanocomposites representing several structural types. (c) Fluorescence intensity decay and (d) emission profile of PbS/TiO$_2$ heterostructures comprising 4.2 nm PbS NCs.
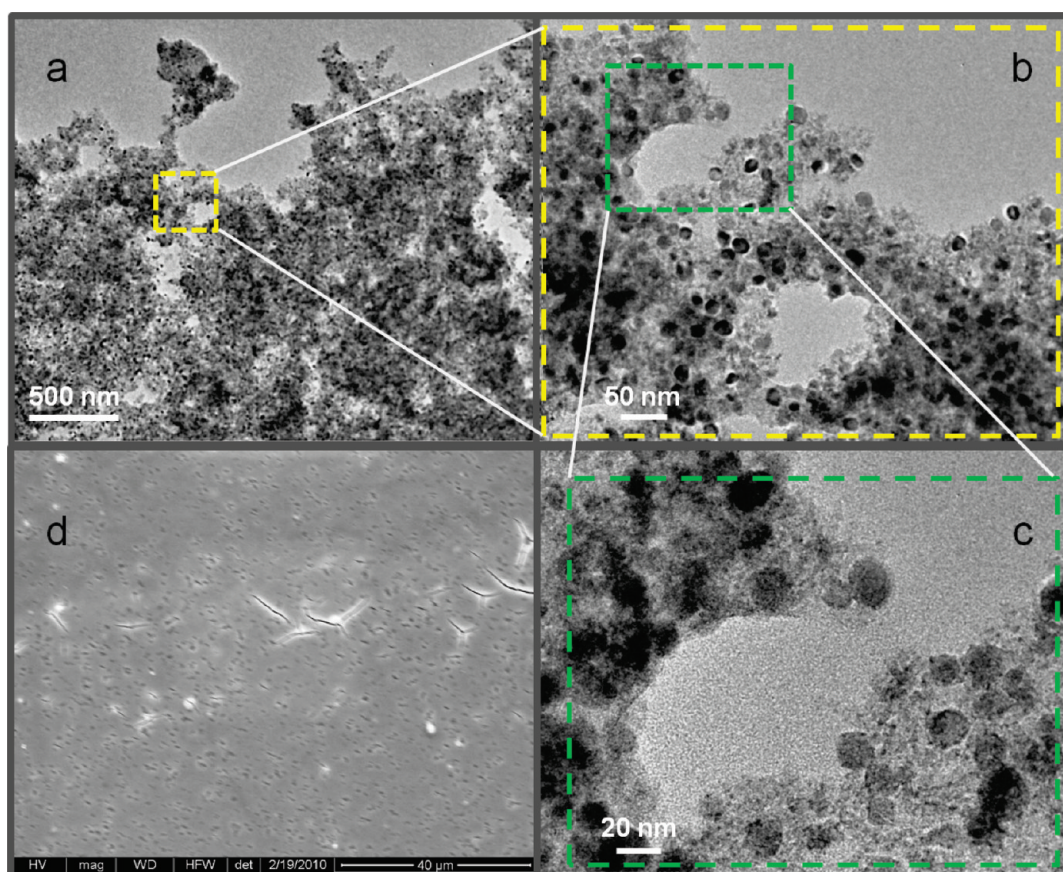

Figure 6. (a) TEM images of pyridine-coated PbS/TiO$_2$ nanocomposites comprising large diameter PbS NCs (d = 18.1 nm). (b,c) Progressive zoom of a selected area in part a from left to right. (d). Scanning electron microscope image of a PbS/TiO$_2$ film on ITO substrate after annealing at 250 °C.

PbS/TiO$_2$ films fabricated in this work was tested using an available but somewhat corrosive polysulfide redox couple (see the Experimental Section), which tends to oxidize PbS NCs. Therefore, as an alternative to measuring absolute efficiencies, the evaluation of the cell performance was done by comparing the PC of PbS/TiO$_2$ nanocomposite-based cells with that of photochemical cells prepared via CBD from nanocrystalline TiO$_2$ (Degussa P-25). All measurements were conducted immediately upon cell fabrication to avoid material degradation due to electrolyte exposure. Preparation of PbS-modified TiO$_2$ electrode through a six-cycle CBD process for comparative studies was done according to ref 69 and is described in the Experimental Section and Supporting Information.

Figure 7a compares the PC spectra of the two cells fabricated from the reported PbS/TiO$_2$ nanocomposite films (red curve) and TiO$_2$ NP films (P25, Degussa) with CBD-grown PbS NCs (blue curve). The signal from pure TiO$_2$ is also shown for comparison. According to Figure 7a, PCs of both cells span the entire visible spectrum and have similar magnitudes throughout the illumination range. Several additional tests performed on other cell pairs confirmed the proximity of the PC values between the two types of devices, implying similar conversion efficiencies. Owing to the fact that the deposition of reported PbS/TiO$_2$ nanocomposite paste was not optimized and the film itself absorbed <45% of incident light at λ = 500% (in contrast with P25 TiO$_2$ films that absorb >95%), the observed PC response was found to be encouraging. Furthermore, it should be noted that the highest value of PC from nanocomposite films was achieved using a relatively low annealing
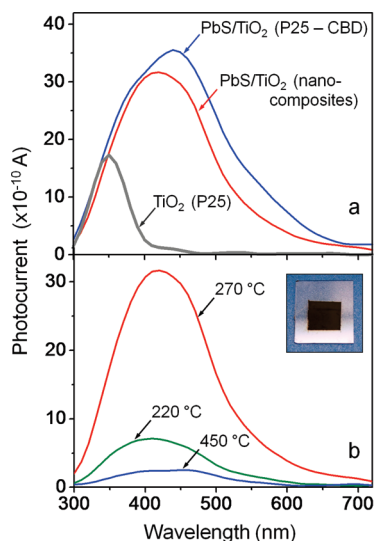
Synthesis of PbS/TiO$_2$ Colloidal Heterostructures

J. Phys. Chem. C, Vol. 114, No. 29, 2010 **12503**

Figure 7. (a) Comparison of the two photocurrent measurements obtained using PbS/TiO$_2$ nanocomposite films (red curve) and PbS-modified P25 TiO$_2$ films fabricated via chemical bath deposition technique (blue curve). Photocurrent measurement from pure TiO$_2$ films on ITO-covered glass is also shown (gray curve). (b) Effect of the annealing temperature on the photocurrent of PbS/TiO$_2$ nanocomposite films. The inset shows an annealed film of PbS/TiO$_2$ heterostructures on ITO-covered glass that performed a working electrode function in fabricated photoelectrochemical cells.

temperature (270 °C), as shown in Figure 7b, which is 180° below the annealing temperature required to sinter P25 TiO$_2$ NP films.

In conclusion, we demonstrated a colloidal synthesis of PbS/TiO$_2$ nanocomposites comprising near-epitaxial assemblies of PbS NCs and TiO$_2$ NRs that can be deployed for the development of solution-processed photovoltaic devices. The size of PbS domains can be tuned from 2 to 20 nm using standard methods of colloidal synthesis, which provides experimental means for optimizing the rates of carrier injection into oxide domains. We found that nanocomposite films comprising 5 nm PbS NCs and annealed at 270 °C enable the highest value of the PC, whereas the photoresponse of films containing large-diameter PbS NCs ($d > 10$ nm) is essentially zero. Light-harvesting characteristics of PbS/TiO$_2$ nanocomposites are explored using an alternative architecture of NC-sensitized solar cells, which provides a facile method to combine high-quality colloidal nanocrystals with an all-inorganic donor−acceptor interface. In light of the renewed interest in NC-sensitized solar cells driven by ongoing research and discovery of noncorrosive and longer-lasting hole scavenging materials, the demonstrated heteroepitaxial PbS/TiO$_2$ films could potentially pave the way for the development of high-performance light-harvesting devices.

Supporting Information Available: Experimental details, statistical distributions of PbS diameters, and additional TEM and HR-TEM images. This material is available free of charge via the Internet at http://pubs.acs.org

References and Notes

(1) Huynh, W. U.; Dittmer, J. J.; Alivisatos, A. P. *Science* **2002**, *295*, 2425.

(2) Huynh, W. U.; Dittmer, J. J.; Teclemariam, N.; Milliron, D. J.; Alivisatos, A. P.; Barnham, K. W. J. *Phys. Rev. B* **2003**, *67*, 115326.

(3) Huynh, W. U.; Dittmer, J. J.; Libby, W. C.; Whiting, G. L.; Alivisatos, A. P. *Adv. Funct. Mater.* **2003**, *13*, 73.

(4) Sun, B. Q.; Marx, E.; Greenham, N. C. *Nano Lett.* **2003**, *3*, 961.

(5) Gunes, S.; Neugebauer, H.; Sariciftci, N. S.; Roither, H.; Kovalenko, M.; Pillwein, G.; Heiss, W. *Adv. Funct. Mater.* **2006**, *16*, 1095.

(6) Fritz, K. P.; Guenes, S.; Luther, J.; Kumar, S.; Saricifitci, N. S.; Scholes, G. D. *J. Photochem. Photobiol., A* **2008**, *195*, 39.

(7) Huynh, W. U.; Peng, X. G.; Alivisatos, A. P. *Adv. Mater.* **1999**, *11*, 923.

(8) Beek, W. J. E.; Wienk, M. M.; Janssen, R. A. J. *Adv. Funct. Mater.* **2006**, *16*, 1112.

(9) Beek, W. J. E.; Wienk, M. M.; Janssen, R. A. J. *Adv. Mater.* **2004**, *16*, 1009.

(10) Greenham, N. C.; Peng, X. G.; Alivisatos, A. P. *Phys. Rev. B* **1996**, *54*, 17628.

(11) McDonald, S. A.; Konstantatos, G.; Zhang, S. G.; Cyr, P. W.; Klem, E. J. D.; Levina, L.; Sargent, E. H. *Nat. Mater.* **2005**, *4*, 138.

(12) Gunes, S.; Fritz, K. P.; Neugebauer, H.; Sariciftci, N. S.; Kumar, S.; Scholes, G. D. *Sol. Energy Mater. Sol. Cells* **2007**, *91*, 420.

(13) Maria, A.; Cyr, P. W.; Klern, E. J. D.; Levina, L.; Sargent, E. H. *Appl. Phys. Lett.* **2005**, *87*, 213112.

(14) Zhang, S.; Cyr, P. W.; McDonald, S. A.; Konstantatos, G.; Sargent, E. H. *Appl. Phys. Lett.* **2005**, *87*, 233101.

(15) Kim, S. J.; Kim, W. J.; Cartwright, A. N.; Prasad, P. N. *Appl. Phys. Lett.* **2008**, *92*, 191107.

(16) Wu, Y.; Wadia, C.; Ma, W. L.; Sadtler, B.; Alivisatos, A. P. *Nano Lett.* **2008**, *8*, 2551.

(17) Mitzi, D. B.; Yuan, M.; Liu, W.; Kellock, A. J.; Chey, S. J.; Deline, V.; Schrott, A. G. *Adv. Mater.* **2008**, *20*, 3657.

(18) Guo, Q.; Kim, S. J.; Kar, M.; Shafarman, W. N.; Birkmire, R. W.; Stach, E. A.; Agrawal, R.; Hillhouse, H. W. *Nano Lett.* **2008**, *8*, 2982.

(19) Koleilat, G. I.; Levina, L.; Shukla, H.; Myrskog, S. H.; Hinds, S.; Pattantyus-Abraham, A. G.; Sargent, E. H. *ACS Nano* **2008**, *2*, 833.

(20) Sargent, E. H. *Adv. Mater.* **2008**, *20*, 3958.

(21) Klem, E. J. D.; MacNeil, D. D.; Levina, L.; Sargent, E. H. *Adv. Mater.* **2008**, *20*, 3433.

(22) Law, M.; Beard, M. C.; Choi, S.; Luther, J. M.; Hanna, M. C.; Nozik, A. J. *Nano Lett.* **2008**, *8*, 3904.

(23) Luther, J. M.; Law, M.; Beard, M. C.; Song, Q.; Reese, M. O.; Ellingson, R. J.; Nozik, A. J. *Nano Lett.* **2008**, *8*, 3488.

(24) Gerischer, H.; Lubke, M. *J. Electroanal. Chem.* **1986**, *204*, 225.

(25) Robel, I.; Subramanian, V.; Kuno, M.; Kamat, P. V. *J. Am. Chem. Soc.* **2006**, *128*, 2385.

(26) Gorer, S.; Hodes, G. *J. Phys. Chem.* **1994**, *98*, 5338.

(27) Niitsoo, O.; Sarkar, S. K.; Pejoux, C.; Ruhle, S.; Cahen, D.; Hodes, G. *J. Photochem. Photobiol., A* **2006**, *181*, 306.

(28) Hao, E. C.; Yang, B.; Zhang, J. H.; Zhang, X.; Sun, J. Q.; Shen, S. C. *J. Mater. Chem.* **1998**, *8*, 1327.

(29) Fang, J. H.; Wu, J. W.; Lu, X. M.; Shen, Y. C.; Lu, Z. H. *Chem. Phys. Lett.* **1997**, *270*, 145.

(30) Wijayantha, K. G. U.; Peter, L. M.; Otley, L. C. *Sol. Energy Mater. Sol. Cells* **2004**, *83*, 363.

(31) Mora-Sero, I.; Bisquert, J.; Dittrich, T.; Belaidi, A.; Susha, A. S.; Rogach, A. L. *J. Phys. Chem. C* **2007**, *111*, 14889.

(32) Lee, J. C.; Sung, Y. M.; Kim, T. G.; Choi, H. J. *Appl. Phys. Lett.* **2007**, *91*, 113104.

(33) Prabakar, K.; Takahashi, T.; Nakashima, T.; Kubota, Y.; Fujishima, A. *J. Vac. Sci. Technol., A* **2006**, *24*, 1613.

(34) Lopez-Luke, T.; Wolcott, A.; Xu, L. P.; Chen, S. W.; Wcn, Z. H.; Li, J. H.; De La Rosa, E.; Zhang, J. Z. *J. Phys. Chem. C* **2008**, *112*, 1282.

(35) Yu, P. R.; Zhu, K.; Norman, A. G.; Ferrere, S.; Frank, A. J.; Nozik, A. J. *J. Phys. Chem. B* **2006**, *110*, 25451.

(36) Vogel, R.; Hoyer, P.; Weller, H. *J. Phys. Chem.* **1994**, *98*, 3183.

(37) Hoyer, P.; Konenkamp, R. *Appl. Phys. Lett.* **1995**, *66*, 349.

(38) Plass, R.; Pelet, S.; Krueger, J.; Grätzel, M.; Bach, U. *J. Phys. Chem. B* **2002**, *106*, 7578.

(39) Lee, H. J.; Yum, J.-H.; Leventis, H. C.; Zakeeruddin, S. M.; Haque, S. A.; Chen, P.; Seok, S. I.; Grätzel, M.; Nazeeruddin, M. K. *J. Phys. Chem. C* **2008**, *112*, 11600.

(40) Lee, H.; Leventis, H. C.; Moon, S.-J.; Chen, P.; Ito, S.; Haque, S. A.; Torres, T.; Nüesch, F.; Geiger, T.; Zakeeruddin, S. M.; Grätzel, M.; Nazeeruddin, M. K. *Adv. Funct. Mater.* **2009**, *19*, 2735.

(41) Morgan, N. Y.; Leatherdale, C. A.; Drndic, M.; Jarosz, M. V.; Kastner, M. A.; Bawendi, M. *Phys. Rev. B* **2002**, *66*, 075339.

(42) Jarosz, M. B.; Porter, V. J.; Fisher, B. R.; Kastner, M. A.; Bawendi, M. G. *Phys. Rev. B* **2004**, *70*, 195327.

(43) Vanmaekelbergh, D.; Liljeroth, P. *Chem. Soc. Rev.* **2005**, *34*, 299.

(44) Zeng, H.; Li, J.; Liu, J. P.; Wang, Z. L.; Sun, S. H. *Nature* **2002**, *420*, 395.

(45) Talapin, D. V.; Murray, C. B. *Science* **2005**, *310*, 86.

(46) Soreni-Hararl, M.; Yaacobi-Gross, N.; Steiner, D.; Aharoni, A.; Banin, U.; Millo, O.; Tessler, N. *Nano Lett.* **2008**, *8*, 678.

(47) Oregan, B.; Grätzel, M. *Nature* **1991**, *353*, 737.

(48) Grätzel, M. *J. Photochem. Photobiol., A* **2004**, *164*, 3.

(49) Wang, P.; Zakeeruddin, S. M.; Humphry-Baker, R.; Grätzel, M. *Chem. Mater.* **2004**, *16*, 2694.

(50) Bai, Y.; Cao, Y.; Zhang, J.; Wang, M.; Li, R.; Wang, P.; Zakeeruddin, S. M.; Grätzel, M. *Nat. Mater.* **2008**, *7*, 626.

(51) Schmidt-Mende, L.; Grätzel, M. *Thin Solid Films* **2006**, *500*, 296.

(52) Kirsanova, M.; Nemchinov, A.; Hewa-Kasakarage, N. N.; Schmall, N.; Zamkov, M. *Chem. Mater.* **2009**, *21*, 4305.

(53) Pathan, H. M.; Lokhande, C. D. *Bull. Mater. Sci.* **2004**, *27*, 85.

(54) Peter, L. M.; Riley, D. J.; Tull, E. J.; Wijayantha, K. G. U. *Chem. Commun.* **2002**, 1030.

(55) Robel, I.; Subramanian, V.; Kuno, M.; Kamat, P. V. *J. Am. Chem. Soc.* **2006**, *128*, 2385.

(56) Kongkanand, A.; Tvrdy, K.; Takechi, K.; Kuno, M.; Kamat, P. V. *J. Am. Chem. Soc.* **2008**, *130*, 4007.

(57) Wang, C. J.; Kwon, K. W.; Odlyzko, M. L.; Lee, B. H.; Shim, M. *J. Phys. Chem. C* **2007**, *111*, 11734.

(58) Hyun, B. R.; Zhong, Y. W.; Bartnik, A. C.; Sun, L.; Abruña, H. D.; Wise, F. W.; Goodreau, J. D.; Matthews, J. R.; Leslie, T. M.; Borrelli, N. F. *ACS Nano* **2008**, *2*, 2206.

(59) Yochelis, S.; Hodes, G. *Chem. Mater.* **2004**, *16*, 2740.

(60) Baker, D. R.; Kamat, P. V. *Adv. Funct. Mater.* **2009**, *19*, 805.

(61) Sun, W. T.; Yu, Y.; Pan, H.-Y.; Gao, X.-F.; Chen, Q.; Peng, L. M. *J. Am. Chem. Soc.* **2008**, *130*, 1124.

(62) Murray, C. B.; Norris, D. J.; Bawendi, M. G. *J. Am. Chem. Soc.* **1993**, *115*, 8706.

(63) Wang, P.; Zakeeruddin, S. M.; Moser, J.-E.; Grätzel, M. *J. Phys. Chem. B* **2003**, *107*, 13280.

(64) Lee, H. J.; Chen, P.; Moon, S.-J.; Sauvage, F.; Sivula, K.; Bessho, T.; Gamelin, D. R.; Comte, P.; Zakeeruddin, S. M.; Il Seok, S.; Grätzel, M.; Nazeeruddin, M. K. *Langmuir* **2009**, *25*, 7602.

(65) Buonsanti, R.; Grillo, V.; Carlino, E.; Giannini, C.; Curri, M. L.; Innocenti, C.; Sangregorio, C.; Achterhold, K.; Parak, F. G.; Agostiano, A.; Cozzoli, P. D. *J. Am. Chem. Soc.* **2006**, *128*, 16953.

(66) Acharya, K. P.; Alabi, T. R.; Schmall, N.; Hewa-Kasakarage, N. N.; Kirsanova, M.; Nemchinov, A.; Khon, E.; Zamkov, M. *J. Phys. Chem. C* **2009**, *113*, 19531.

(67) Seo, J.; Jun, Y.; Ko, S.; Cheon, J. *J. Phys. Chem. B* **2005**, *109*, 5389.

(68) Zhang, D. S.; Yoshida, T.; Oekermann, T.; Furuta, K.; Minoura, H. *Adv. Funct. Mater.* **2006**, *16*, 1228.

(69) Lee, H.; Leventis, H. C.; Moon, S.; Chen, P.; Ito, S.; Haque, S. A.; Torres, T.; Nü esch, F.; Geiger, T.; Zakeeruddin, S. M.; Grä tzel, M.; Nazeeruddin, M. D. *Adv. Func. Mater.* **2009**, *19*, 2735.

(70) Lee, Y. L.; Chang, C. H. *J. Power Sources.* **2008**, *185*, 584.

(71) *Crystal Growth for Beginners: Fundamentals of Nucleation, Crystal Growth, and Epitaxy*; Markov, I. V., Ed.; World Scientific: Singapore, 2003.

(72) Wehrenberg, B. L.; Guyot-Sionnest, P. *J. Am. Chem. Soc.* **2003**, *125*, 7806.

(73) Wei, S. H.; Zunger, A. *Phys. Rev B* **1997**, *55*, 13605.

(74) Hewa-Kasakarage, N. N.; Kirsanova, M.; Nemchinov, A.; Schmall, N.; El-Khoury, P. Z.; Tarnovsky, A. N.; Zamkov, M. *J. Am. Chem. Soc.* **2009**, *131*, 1328.

(75) Du, H.; Chen, C. L.; Krishnan, R.; Krauss, T. D.; Harbold, J. M.; Wise, F. W.; Thomas, M. G.; Silcox, J. *Nano Lett.* **2002**, *2*, 1321.

(76) Murray, C. B.; Norris, D. J.; Bawendi, M. G. *J. Am. Chem. Soc.* **1993**, *115*, 8706.